Role and Dynamics of Transition Metal Carbides in Methane Coupling

Seraphine B.X.Y. Zhang,[1] Quentin Pessemesse, [2] Lukas Lätsch,[1] Konstantin M. Engel,[1]
Wendelin J. Stark,[1] Alexander P. van Bavel,[3] Andrew D. Horton,[3] Pierre-Adrien Payard,[2,*]
Christophe Copéret[1,*]

[1]Department of Chemistry and Applied Biosciences, ETH Zurich, Vladimir-Prelog-Weg 2, 8093 Zurich

[2] Université Claude Bernard Lyon I, CNRS, INSA, CPE, UMR 5246, ICBMS, 1 rue Victor Grignard, 69622 Lyon

[3]Shell Global Solutions International B.V., Grasweg 31, 1031 HW Amsterdam

* pierre-adrien.payard@univ-lyon1.fr; ccoperet@ethz.ch

Transition metal carbides have numerous applications and are known to excel in terms of hardness, thermal stability and conductivity.[1] In particular, the Pt-like behavior of Mo and W carbides[2,3] has led to a popularization of metal carbides in catalysis, ranging from electrochemically-driven reactions[4] to thermal methane coupling.[5,6,7] Herein, we show the dynamics of Mo and W carbides and the active participation of carbidic carbon in the formation of C_2 products during methane coupling. A detailed mechanistic study reveals that the catalyst performance of these metal carbides can be traced back to its carbon diffusivity and exchange capability upon interaction with gas phase carbon (methane). A stable C_2 selectivity over time on stream for Mo carbide (Mo_2C) can be rationalized by fast carbon diffusion dynamics, while W carbide (WC) shows loss of selectivity due to slow diffusion leading to surface carbon depletion. This finding showcases that the bulk carbidic carbon of the catalyst plays a crucial role and that the metal carbide is not only responsible for methyl radical formation. Overall, this study supports the presence of a carbon equivalent to the Mars-Van Krevelen type mechanism for non-oxidative coupling of methane, thus introducing guiding principles to design and develop associated catalysts.

Main

Transition metal carbides are ubiquitous in catalysis today, particularly in the context of C-H activation.[8,9] While molybdenum and tungsten are prominent metals in state-of-the-art catalysts for oxidative and non-oxidative coupling of methane,[10,11] MoO_x/ZSM-5 has become the gold standard for methane coupling to aromatics.[10,12] For this system a characteristic induction period along with particle agglomeration is observed which is rationalized by a transformation of the molybdenum oxide to the corresponding oxycarbide or carbide species which is presumed to resemble the active species in methane coupling.[13,14,15,16] Yet, the mechanism for non-oxidative coupling of methane is still a matter of debate. High reaction temperatures, i.e. in the range of 800-1100°C, suggest the involvement of radical pathways in the gas phase and the catalyst activity is often ascribed to methyl radical formation which then form C_2 products downstream of the catalyst bed.[17,18,19] Previous reports addressing the involvement of carbidic carbon in metal carbide catalysts[20,21] prompted us to investigate the role of carbon closer in bulk Mo and W carbides (Mo_2C and WC) by applying a ^{13}C-labelling strategy combined with several spectroscopic techniques (XPS, ss-NMR, pXRD) and metadynamics simulations to illuminate the mechanistic aspects in methane coupling. Mo and W carbides were tested as catalysts for the non-oxidative methane coupling (NOCM). Both materials enable C_2 product formation at 1100°C with 21% C_2 selectivity at 23 % CH_4 conversion for Mo_2C (4.7 % C_2 yield) and 32% C_2 selectivity at 10% CH_4 conversion for WC (3.2% C_2 yield). Furthermore, this study shows that carbidic carbon participates in C_2 product formation and interacts with gas phase carbon (methane). Differences in methane coupling activity could be rationalized by investigating surface composition with XPS and carbon diffusion coefficients by metadynamics at the DFT level. Following the analysis, we concluded fast C exchange dynamics for Mo_2C and slow C diffusion for WC. The incorporation of carbon originating from methane was

evidenced by ss-NMR of the spent materials with carbidic carbon NMR signatures at 274 ppm and 307 ppm for Mo_2C and WC, respectively. Hence, this study supports the participation of a carbon equivalent to the Mars-Van Krevelen type mechanism in non-oxidative coupling of methane, which is typically encountered in oxidation processes with certain metal oxides.[22,23]

Synthesis and Activity of Transition Metal Carbides

Mo_2C and WC were prepared via carburization at 1000 °C, and their catalytic activity in NOCM investigated (Fig. 1). They were characterized with pXRD, XPS and TEM. Detailed synthesis procedures, characterization and catalytic test conditions for Mo_2C and WC can be found in the methods section and the SI. Unless otherwise stated, all data sets are averages of 1-hour time on stream (TOS) at a given temperature. At 1100°C, Mo_2C and WC convert methane to C_2 products and coke with C_2 yields of 4.7% for Mo_2C and 3.2% for WC (Fig. 1a). For Mo_2C, methane conversion increases with temperature: from 9.7% at 900°C to values of up to 23.0% at 1100°C with an average C_2 selectivity of 20.6% which is stable over time on stream. In the case of WC, methane conversion reaches a maximum of 9.6% at 1100°C with a C_2 selectivity of 32.5%, while a loss of selectivity is observed over time on stream. Comparing both carbides, methane conversion is higher for Mo_2C while the C_2 selectivity is higher for WC. It is also noteworthy that at 900°C WC already converts methane, albeit with a low C_2 selectivity of 3.2% while no C_2 products are detected for Mo_2C. The best selectivity towards C_2 products between the two catalysts was determined as 32.5% at 9.9% methane conversion for WC at 1100°C, albeit the latter suffers from a fast deactivation.

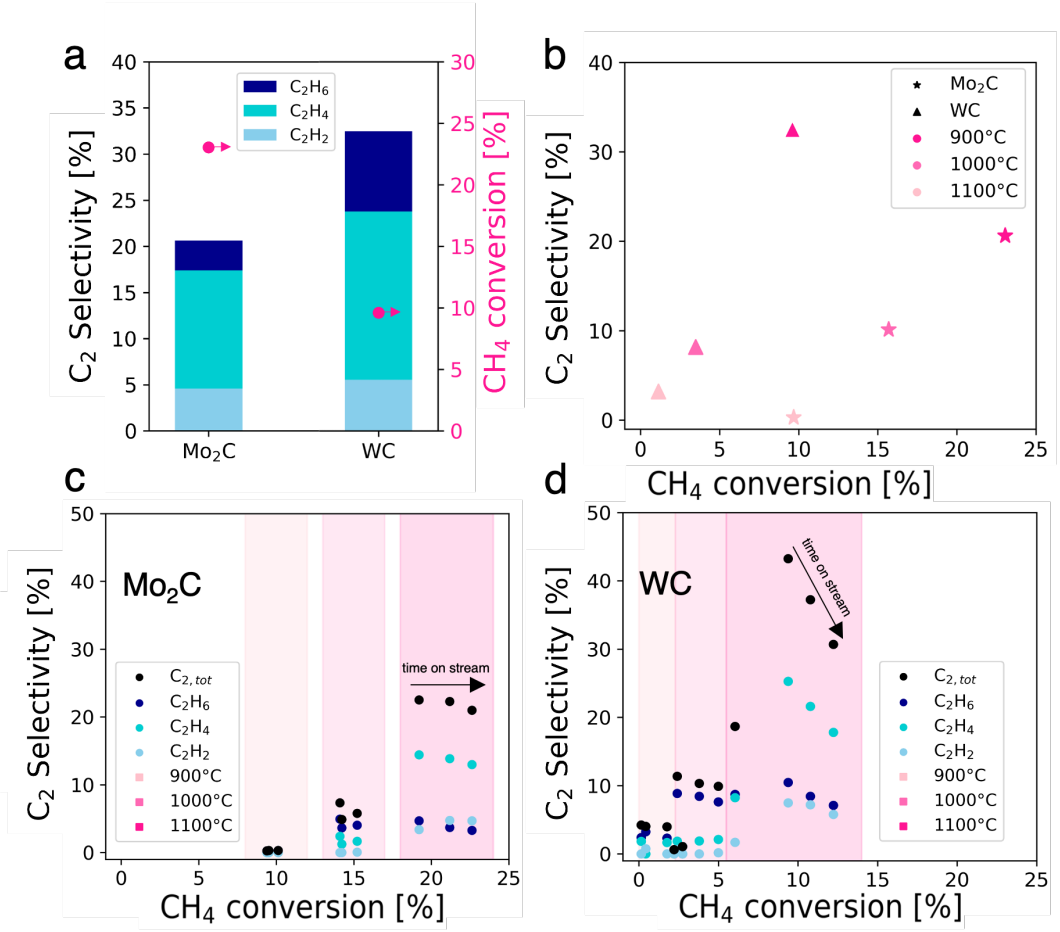

Fig. 1: a Selectivity distribution for C_2 species and CH_4 conversion at 1100 °C with 10% CH_4 in Argon for Mo_2C and WC (averaged over 1h time on stream). **b** Effect of reaction temperatures on the C_2 selectivity and CH_4 conversion for the different catalysts. The color indicates the temperature and the form the catalyst. CH_4 conversion vs C_2 selectivity at 900, 1000 and 1100°C for C_2 species over time on stream for **c** Mo_2C and **d** WC; data points were taken every 15 min.

In general, the highest conversion levels and C_2 selectivities are obtained at high temperatures (Fig. 1b). Mo_2C on the one hand exhibits stable selectivity at increasing conversion during time on stream at 1100°C, forming coke and aromatics as major reaction byproducts (Fig. 1c). WC on the other hand experiences rapid loss of C_2 selectivity over time on stream at 1100 °C along with increasing methane conversion (Fig. 1d).

Role of Carbon in Mo and W Carbides

The evolution of Mo_2C and WC materials was furthermore investigated by comparing the materials before and after NOCM (3h on stream at 900, 1000 and 1100°C, 1h at each temperature) using pXRD and XPS (Fig. 2). Based on pXRD, the bulk structures of Mo and W carbides remain unchanged for pristine and spent catalysts. XPS gives insight regarding differences in surface composition, namely carbon (surface) depletion for WC and structural retention for Mo_2C. In the case of Mo_2C, two components of the 3d 5/2 peak are observed at binding energies of 228.6 and 229.4 eV associated with Mo^{2+} (Mo_2C) and Mo^{4+} (MoC or MoO_2), respectively.[13,14,24] This finding remains unchanged considering pristine and spent catalyst surface. For WC, the XPS spectra (Figure 3d) can be fitted as two multiplets that correspond to the W 4f 7/2 and W 4f 5/2 components which have a spin-orbit splitting of 2.2 eV. The WC (W^{4+}) peaks were identified at 32.5 and 32.7 eV for the pristine and the spent catalyst, respectively. The W 4f 7/2 peak at 36.6 eV was attributed to WO_3. Pristine WC shows a mixture of WC (32.5 eV) and WO_3 (36.6 eV) on the surface. While no WO_3 was found in the spent WC, reduction to metallic W(0) with the 4f 7/2 component at 32.1 eV was observed. For W(0) metal, a characteristic loss feature is reported,[25] here it can be observed as a broad peak at 38 eV. Overall, XPS measurements show a change in composition for the surface from a mixture of WO_3 and WC in the pristine catalyst to WC and W(0) in the spent catalyst hinting towards carbon depletion on the surface of WC with concomitant reduction to metallic W.

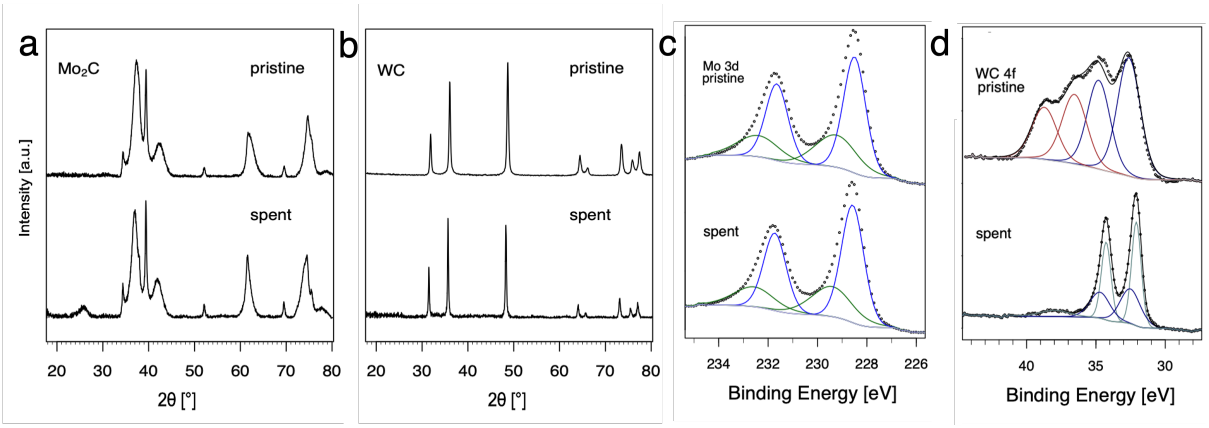

Fig. 2: Structural transformations for pristine and spent catalyst materials are shown. pXRD for (**a**) Mo_2C, (**b**) WC and XPS spectra of pristine and spent metal carbides: (**c**) Mo_2C 3d, (**d**) WC 4f. The dots represent the recorded data and the solid lines show the results of a curve-fitting procedure.

Intrigued by this finding, the reaction of $^{13}CH_4$ with these materials was investigated in order to elucidate the role of surface C in transition metal carbides and to examine whether there is incorporation of the carbide surface C in the final products. $^{13}CH_4$ labelling experiments were performed for Mo_2C and WC in a batch reactor (see Fig. S10). The reactor was filled with the respective metal carbide, 200 mbar of $^{13}CH_4$ at r.t., heated to 1100°C with a heating ramp of 400°C/h and subsequent aliquots were taken after 3, 6, 9 and 12 h. Aliquots of the gas mixture are taken and analyzed with GCMS resulting in mass fragmentation patterns allowing to monitor the distribution of isotopomers among coupling products (non-, mono- and di-labelled C_2 products) for ethane, ethylene and acetylene (see Table S2 and Fig. S7). The degree of carbidic ^{12}C incorporation into C_2 products was investigated by monitoring product evolution over the course of 12h, with aliquots drawn every 3 hours (Fig. 3 a,b). In the case of Mo_2C, the isotopomer distribution is dominated by non-labelled C_2 products, with ethane and ethylene as major gaseous products. The isotopomer distribution among ethane (Fig. 3 a) is dominated by the non-labelled C_2H_6 (93%) after 3 hours, with mono- and di-labelled C_2H_6 being at 6% and 1%, respectively. The ratios of isotopomers change slightly

with time; the amount of non-labelled C_2H_6 reaches 89% along with 7 and 4% of mono- and di-labelled isotopomers after 12h. This finding suggests the incorporation of carbidic carbon in C_2 products and C mobility in the Mo_2C matrix. Considering that the surface and the bulk of Mo_2C remains unchanged according to XPS and pXRD analysis, this labelling study further suggests fast C exchange with gas phase $^{13}CH_4$ resulting in rapid reformation of the Mo_2C and thus allows for maintaining a constant product selectivity. The exchanged carbidic C is replenished with ^{13}C from the gas phase explaining the increase in labelled products over time.

For WC (Fig. 3b), ethylene is formed as major gaseous product under the same reaction conditions. However, in sharp contrast to Mo_2C, the amount of di-labelled C_2H_4 isotopomer dominates (97%) for WC, with only a minor fraction of non- (1%) and mono-labelled (2%) C_2H_4 after 3h. With increasing reaction time and conversion of $^{13}CH_4$, the relative amount of ^{12}C isotopomer increases with mono- and non-labelled isotopomers C_2H_4 reaching 14% and 9%, respectively after 12h, indicating that WC can also act as a source of carbon, albeit much less efficiently than Mo_2C. As discussed above, this process is accompanied by a reduction over time of WC to W(0) as evidenced by XPS (Fig. 2d), indicating a C depletion of the WC matrix. This change in catalyst state and the presence of metallic W offers a possible explanation for the loss of selectivity over time on stream with simultaneous increase in methane conversion.

Considering the sharp contrast of reactivity patterns in these carbides (observed in presence of labelled methane), one might pose the question whether Mo_2C and WC can release carbon in the form of methane by interaction with H_2 (10% H_2 in Ar, 40 mL/min, up to 1100 °C). As expected from their different carbon mobility (vide infra),methane evolution could only be observed for Mo_2C (see Fig. S23).

In order to study ^{13}C enrichment in the spent materials by exchange between the surface ^{12}C of the carbide and the gas phase $^{13}CH_4$, the materials were further examined by ^{13}C MAS NMR (Fig. 3 c,d). It should be noted that good quality spectra could only be obtained when diluting the sample with KBr. While hardly any signal is observed on pristine materials, in particular for Mo_2C, intense signals are observed post-reaction, consistent with the exchange of carbon between the gas phase and the solid. For both WC and Mo_2C, two peaks are observed, corresponding to the carbidic carbon and sp^2 carbon signals (graphitic carbon), the former appearing at 307 ppm for WC and at 274 ppm for Mo_2C. The ^{13}C shift of Mo_2C agrees with previous reports,[15] while the spectrum of WC has to date not been reported to the best of our knowledge.

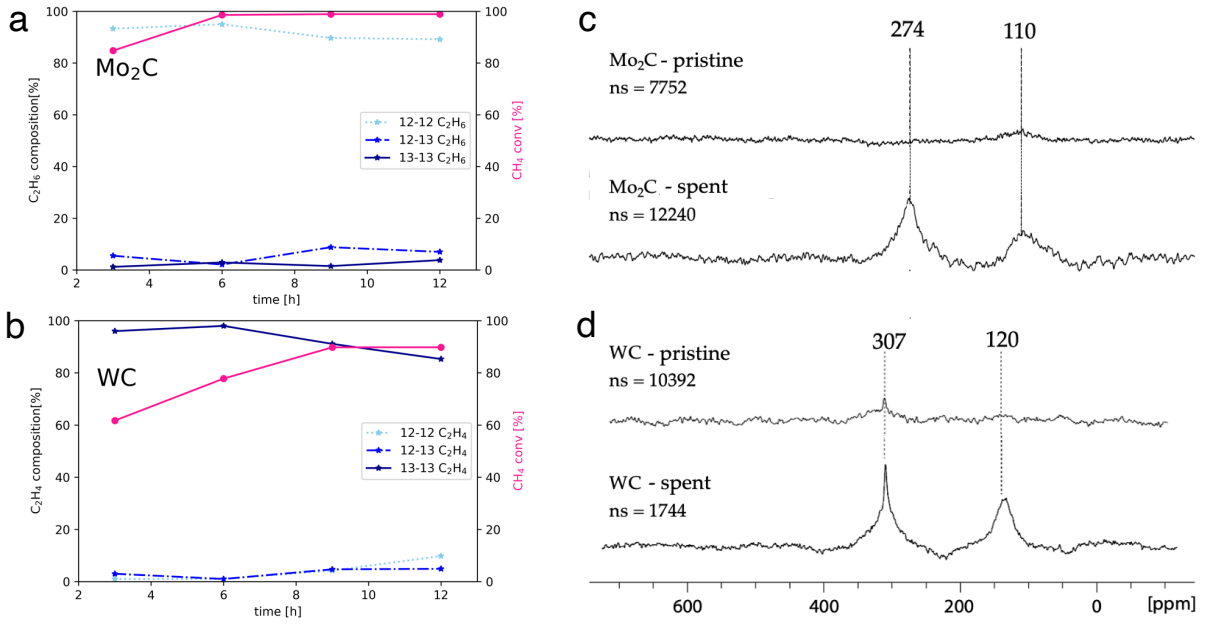

Fig. 3: Left: Product distribution for dilabelled, monolabelled and non-labelled C_2 products in case of Mo_2C (**a**) and WC (**b**) as a function of contact time. Right: ^{13}C MAS NMR characterization of pristine and spent (**c**) molybdenum carbide (Mo_2C) and (**d**) tungsten carbide (WC). The catalyst was contacted with 200 mbar $^{13}CH_4$ in batch for 24 h at 1100 °C.

One may note that the sp^2 carbons have different chemical shifts for WC and Mo_2C, indicating the presence of different types of carbons, possibly aromatic carbon deposit around 120 ppm vs. graphitic carbon around 110 ppm for WC and Mo_2C, respectively.[26,27] Summarizing these findings, the incorporation of surface/carbidic ^{12}C from the carbide in the C_2 products was shown for both Mo_2C and WC, yet Mo_2C exhibits a significantly higher C mobility of the carbide matrix than WC. The faster exchange/diffusion of carbidic carbon or the formation of methane from Mo_2C are possible rationales for these contrasting isotopomer distributions.

Modelling Diffusion of Carbon in Mo_2C and WC

In order to better understand the carbon exchange capability of molybdenum and tungsten carbides, the diffusion mechanism of carbon in the matrix at 1100°C was explored using metadynamics at the DFT level (see the computational details for the method used).[28,29,30,31,32] The diffusion of a single carbon atom through a periodic cell of Mo_2C and WC was investigated. The (001), (010) and (011) facets were considered to account for the anisotropy of the material; diffusion mechanisms and diffusion coefficients were similar in all cases so that only the (010) case will be discussed in the following, see SI section 7 for facets (001) and (011) and computational details. The cells consist of 6-atom layers with two fixed bottom layers.

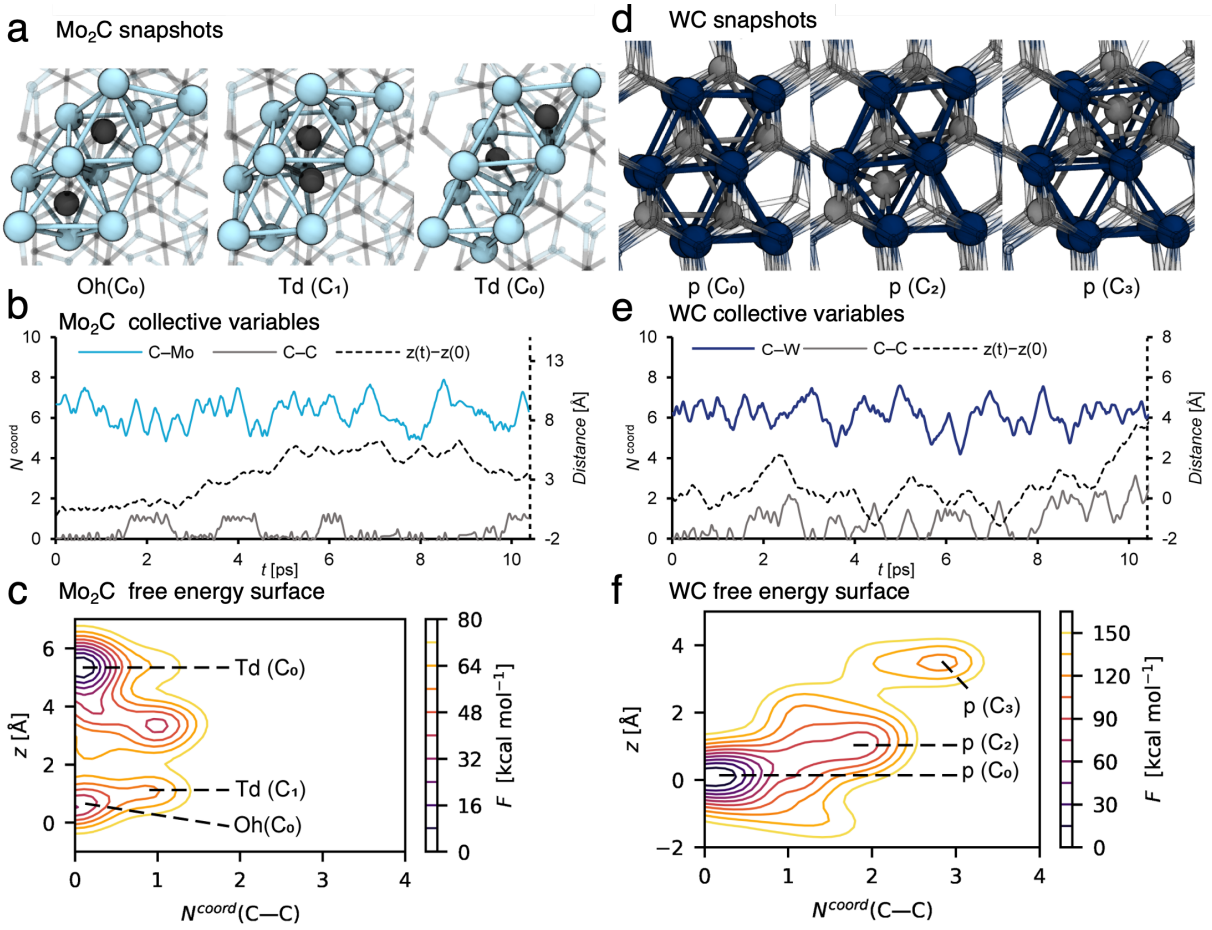

Fig. 4 Successive sites involved in the diffusion of carbon towards the (010) facet in Mo_2C (**a** octahedral O_h and tetrahedral T_d sites with (C_1) or without C-C interaction (C_0)) and WC (**d** prismatic sites p with x C neighbors C_x). Biased collective variables as a function of the simulation time for the diffusion of carbon in Mo_2C (**b**) and in WC (**e**). Free-energy surfaces as a function of the coordination number from C to C (N^{coord}(C-C)) and distance along the *z* axis with respect to the initial position (*z*) for Mo_2C (**c**) and WC (**f**).

A potential bias was applied along selected collective variables, namely: the vertical position of the C atom (*z*), the C-C and C-M coordination numbers, N_{coord}(C-C) and N_{coord}(C-M) respectively, to accelerate diffusion. The free energy surfaces associated to *z* and N_{coord}(C-C) were reconstructed by summing up the energy bias. The calculated

free energy barrier (Fig. 4c, from z = 0.5 Å to z = 5.5 Å) to diffuse from the resting site to a higher lying site in Mo_2C is ~ 40 kcal mol^{-1}, which corresponds to a diffusion coefficient of D_{Mo2C}^{1373K}= 1.3 x 10^{-11} m^{2}s^{-1} at 1100°C. This value suggests that carbon diffuses very easily in the bulk at this temperature with an order of magnitude of the diffusion coefficient similar to the one obtained at ambient temperature for organic molecules in a liquid phase.[33] The carbon diffusion in Mo_2C takes place through migration of a C atom from a resting octahedral site (O_h) to vacant tetrahedral (T_d) ones (Fig. 4a). As evidenced by the variation of the collective variables with time (Fig. 4b), two different tetrahedral sites are present in the crystal structure leading either to an isolated tetrahedral carbide (N_{coord}(C-C) = 0, Fig. 4a, Td(C_0)) or to the formation of a C_2 moiety with an adjacent octahedral C neighbor (N_{coord}(C-C) = 1, Fig. 4a, Td(C_1)). In the latter, distortion of the crystal structure may lead to the formation of C_2 defects with neighboring carbon sites, slowing down migration through these sites. As indicated by the free energy surface (FES, Figure 6c, N_{coord}(C-C) = 1)), C_2 defects are easily formed at this temperature and are likely to be involved in the subsequent formation of the coupling products. The contrasting behavior for WC reoccurs as the calculated diffusion of carbidic carbon in WC is significantly slower. The calculated free energy barrier for diffusion in WC (Fig. 4f between z = 0 Å and z = 4 Å) and the associated diffusion coefficient are ~140 kcal mol^{-1} and D_{WC}^{1373K} = 7.5 x 10^{-30} m^2 s^{-1}, respectively. For WC, carbon has to move through surrounding unoccupied prismatic sites (Fig. 4d, p(C_2) and p(C_3)), and interacts with the carbon atoms occupying the neighboring prismatic sites (Fig. 4e, N_{coord}(C-C) > 0), leading to the formation of transient C_x moieties (x = 3 and 4, Fig. 4e,f). The difference in calculated diffusion coefficients of around 20 orders of magnitude between Mo_2C and WC is in agreement with the distribution of C_2 products, which contain mainly non-labelled species originating from the ^{12}C-bulk in the case of Mo_2C, and mainly di-labelled species originating from the $^{13}CH_4$ reactant gas in the case of WC. These results further confirm what was observed by XPS (vide supra). In WC, carbon diffusion is slow and carbon depletion is not compensated by incorporation of carbon from gas phase methane, thus leading to formation of metallic W(0). In the case of Mo_2C, carbon easily diffuses through the bulk and is replenished rapidly at the surface as the spent catalyst's XPS signature resembles the pristine one.

Discussion

Based on the significant amount of ^{12}C-containing C_2 products, a Mars-Van Krevelen type mechanism[23] with participation of carbidic carbon of the metal carbide (instead of oxygen in a metal oxide) is most suited to rationalize our findings as illustrated in the mechanistic proposal shown in Fig. 5. The activation step can follow two possible mechanisms depending on the carbon mobility of the parent carbide. For carbides with higher carbon diffusion coefficients like Mo_2C, one can propose (pathway a) that two carbon atoms recombine to form a C_2 unit and desorb as ethane by combining with hydrogen atoms adsorbed on the surface (H_{ads}); this explains the absence of labelling of the hydrocarbon products at the initial stage, the labelling of the carbide without its reduction and the incorporation of ^{13}C with increasing time.

With decreasing carbon mobility like for WC, the formation of products involves surface reactions (pathway b), where C-H activation can form surface hydrocarbyls (alkyl, alkylidene and alkylidines) as previously proposed.[34,35] Pathway (b) comprises two subsequent C-H activations on the metal carbide which yields a methylidene species which then further interacts with a non-labelled surface C releasing mono-labelled ethane, facilitated by H_{ads}. During the propagation, carbon-13 is restored on the metal carbide surface releasing di-labelled products. The origin of ethylene and acetylene can be either rationalized by thermolytic dehydrogenation or catalytic formation via the carbide pathway on the surface. At longer reaction times the fraction of labelled products decreases due to consumption of $^{13}CH_4$. At several states in this catalytic cycle, the carbidic carbon on the surface can be regenerated by diffusion through the bulk or by interaction with methane in the gas phase. While pathway a or b might be more pronounced for certain metal carbides, it is most likely a combination thereof.

This mechanistic proposal is consistent with our data and previous findings, i.e. (i) C_2H_6 is the proposed primary product,[36] (ii) H_{ads} diffuses over the surface rapidly[34] and (iii) alkylidene species can be formed on metal carbide surfaces.[6,34,37,38] Similar findings have been proposed in the Fischer-Tropsch process based on Fe carbide[39] or for the

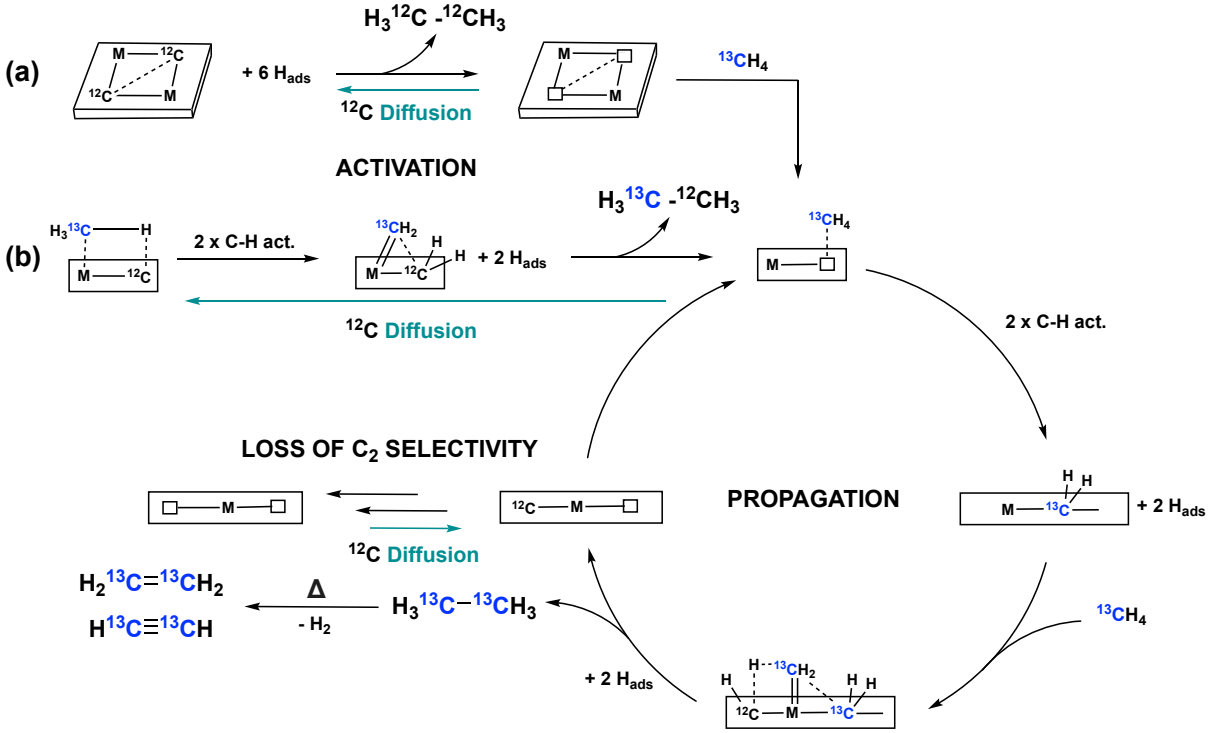

Fig. 5 Proposed mechanism for non-oxidative CH_4 coupling on transition metal carbide surfaces. M= Mo or W. Deactivation was exclusively observed for W.

methane aromatization on WC_x clusters on ZSM-5.[40] While the surface is enriched in carbon-13 as evidenced by NMR, the low mobility of carbon leads to a depletion in carbon at the surface and the formation of W(0), explaining the faster loss of C_2 selectivity of W carbide. Additionally, considering that carbon mobility increases with temperature, the rise in conversion as well as C_2 selectivity at elevated temperatures (Fig. 1b) can be accounted for. While methane coupling is mechanistically mostly rationalized by radical coupling pathways with the methyl radical as initiator,[17,18] this study shows that alternative mechanistic pathways are possible and greatly depend on the nature/structure of the metal carbides, which control the mobility and diffusivity of carbon.

Conclusions

In this study, the crucial role of carbidic carbon in the active catalytic materials was shown by (i) incorporation of carbidic carbon in C_2 products, (ii) reduction of WC to W(0) leading to lower product selectivity, (iii) ^{13}C exchange between gaseous methane and Mo/W carbide surfaces as evidenced by ss-NMR and (iv) computation of carbon diffusion coefficients in Mo and W carbides. For Mo_2C, fast carbon diffusion, as shown by labelling studies and computations, allows replenishment of the surface and a good catalytic performance (stable selectivity). In sharp contrast, under the same conditions, WC undergoes reduction of the surface species to W(0), consistent with the significantly lower fraction of carbidic carbon incorporated into the gaseous products and the slower calculated carbon diffusion, probably explaining the fast loss of C_2 product selectivity.

This study supports that a Mars-van Krevelen-like mechanism involving carbon atoms is at play, paralleling what is observed with oxygen and metal oxides in several oxidation reactions.[22,23,41] While more insights in the mechanism of methane coupling are certainly needed to fully understand the product formation processes, this work shows that carbidic carbon and its dynamic behavior plays a crucial role in methane coupling to higher hydrocarbon products; governing selectivity and conversion. This study further highlights that dynamics of metal carbides should be considered more broadly and be integrated as design parameters in catalysis.

Methods

Preparation of materials. WO_3 powder was synthesized by flame spray pyrolysis using WCl_6 in dissolved in THF and benzyl alcohol. 5 mL/min of the latter were dispersed with an oxygen flow of 5 NL/min into a support flame of CH_4/O_2. The resulting nanoparticles were collected on a glass filter. In a second step, WO_3 was carburized in a feed of CH_4/H_2 (20/80 v/v) with a total flow of 40 mL/min at 1000 °C resulting in WC (3 m^2/g) (Fig. S1). Mo_2C nanorods (21 m^2/g) were synthesized as previously reported (Fig. S2).[42] To 2.5 g of ammonium heptamolybdate tetrahydrate ($(NH_4)_6 Mo_7O_{24} \cdot 4 H_2O$) dissolved in 40 mL water containing 3.8 g p-methylaniline was added 1.0 M hydrochloric acid to adjust the pH value to 4.0. After reaction at 50 °C for 4 h, the precipitate was filtered, washed with water and ethanol, and then dried *in vacuo*. The Mo oxide precursor was carburized by transferring into a tube furnace and heated to 1000°C (300°C/h) under argon flow (30 mL/min), the temperature was kept for 1h before cooling down to r.t. More details for the synthesis can be found in the supporting information.

pXRD. X-Ray diffraction of the samples was performed with a STOE STADI P powder diffractometer, operating in transmission mode. A germanium monochromator, Cu $K\alpha_1$ irradiation and Dectris Mythen silicon strip detector were used. β-Mo_2C (PDF # 00-035-0787) and WC (PDF # 00-073-0471) structures were confirmed.

XPS. XPS analysis was performed using the SIGMA II instrument equipped with a Al/Mg twin anode. The vacuum in the chamber was around $2x10^{-8}$ mbar during measurements. The analyses were carried out with a Mg-Kα source (energy = 1253.6 eV, 0.1 eV step size) in LAXPS mode with a pass energy of 16 eV. The curve-fitting was performed with Shirley background and lineshape GL(30). C1s was used for referencing at 284.8 eV.

TEM. Images were recorded using a JEOL JEM- 2200FS microscope operated at 200 kV.

^{13}C solid state MAS NMR. ^{13}C solid state MAS NMR measurements were carried out using a Bruker 400 MHz NMR spectrometer operating at a frequency of 400 MHz. A 4.0 mm MAS NMR zirconia rotor was used with a spinning speed of 10 kHz. A spin echo sequence with a 5 μs $\pi/2$ pulse and a relaxation delay of 7s was applied. The spectra were recorded at room temperature and referenced with adamantane (38.4 ppm).

Catalytic tests. The catalytic tests were conducted in a fixed-bed quartz reactor with a length of 400 mm and an ID of 9 mm (Fig. S8). The temperature program was 900°C-1000°C-1100°C, each temperature was kept for 60 min. The heating rate was 100°C/min in an IR furnace. The standard operating conditions were 0.1 g of catalyst, 10 v% of CH_4 in Argon with a total flow of 40 sccm resulting in a GHSV of 24'000 $mL*g_{cat}^{-1}*h^{-1}$.

Unless otherwise stated, all data sets are averages of 1-hour time on stream (TOS) at a given temperature. As comparison, a blank experiment (empty reactor without catalyst) under the same conditions showed a CH_4 conversion of 4.4% with no selectivity towards the desired products, but only coke deposition. Additionally, it must be mentioned that the product formation towards aromatics could not be quantified (S11).

Experiments with $^{13}CH_4$. 0.5 g of the respective carbide was loaded into a 44 mL quartz glass batch reactor. The reactor was filled with 200 mbar of $^{13}CH_4$ (corresponding to molar ratios of 7.2/1 for WC/$^{13}CH_4$ and 6.9/1 for $Mo_2C/^{13}CH_4$) and heated to 1100°C with a heating ramp of 400°C/h. Aliquots were drawn using a gas-tight syringe after 3, 6, 9 and 12 h (Fig. S10). A gas mixture containing 0.5% acetylene, 5% ethane, 10% ethylene, 10% Helium, 15% H_2, 39.5% Ar and 20% CH_4 was used for calibration. The MS fragmentation patterns of ethane, ethylene and acetylene were used as references for quantification of non-, mono- and di-labelled C_2 products assuming that their fragmentation patterns are shifted by m/z=+1 and m/z=+2, respectively (Fig. S6/7). Reaction monitoring by GC-MS allowed analyzing the distribution of isotopomers (non-, mono- and di-labelled C_2 products) for ethane, ethylene and acetylene (see Table S2 and Fig. S5) by fitting the fragmentation patterns.

Computational Details. *Ab initio* molecular dynamics (AIMD) and metadynamics (MTD) simulations were carried out using the CP2K 5.1 software.[43,44]

Molybdenum (Mo_2C) and tungsten (WC) bulk was modelled using surface slabs constructed using the reported crystalline orthorhombic (Pbcn)[45] and hexagonal (P6m2)[46] structures respectively. Along the vertical axis the 6-layers slabs were separated by a 10 Å layer of vacuum to avoid self-interactions. The bottom layers of atoms were fixed. The size of the cell (~10 x 10 x 20 $Å^3$) was considered large enough to account for the electronic structure of the system.

Each MTD run was preceded by an unbiased AIMD of 2 ps at 1373 K to ensure thermal equilibration. A MD step length of 1 fs was used. The systems evolved in the NVT canonical ensemble equilibrated using a canonical sampling through velocity rescaling (CSVR) thermostat set at 1373 K with a global temperature tolerance of 20 K. The force field was computed using the revised version of the Perdew-Burke-Ernzerhof PBE functional[47,48] and Grimme dispersion correction D3 with Becket-Johnson (BJ) damping function.[49,50] Atoms were described using single-ζ molecularly optimized (MOLOPT) gaussian basis sets[51,52] and associated Goedecker-Teter-Hutter GHT pseudopotential.[53] Molecular orbitals occupation numbers were smeared using the Fermi-Dirac method.

The free energy surface (FES) related to carbon diffusion in the metal carbide phase was explored by means of metadynamics,[28,29,30,31,32] using a history dependent potential applied along selected collective variables (CVs). In addition to the position on the z axis relatively to a plane described by three atoms belonging to the fixed layers, the coordination numbers from C to C and from C to metal (M = Mo or W) were considered:

$$N^{coord}(C-X) = \sum_i \frac{\left(1-\frac{r_i}{R_0}\right)^{nn}}{\left(1-\frac{r_i}{R_0}\right)^{nd}}$$

where nn = 12, nd = 24, and R_0 corresponds to the CX bond distance, and takes 1.6 Å for the C–C bonds and 2.3 Å for the C–M ones.

The gaussian bias takes the following form:

$$V\big(t, s(t)\big) = w \sum_n e^{\frac{-1}{2}\left(\frac{s(t)-s(n\cdot t_G)}{\delta_S}\right)^2}$$

with w = 1 kcal mol^{-1} (Mo_2C) and 2 kcal mol^{-1} (WC) and δ_G = 0.3, respectively, being the height and width of the Gaussian and t_G = 10 fs being the time interval between two consecutive depositions.

The diffusion coefficient at 1373 K were estimated using the following formula:[54]

$$D(T) = \frac{k_B T}{h} l^2 exp\left(\frac{-\Delta F_d(T)}{k_B T}\right)$$

With l the distance traveled by the atom, ΔF_d the free energy of activation, k_B the Boltzmann constant, h the Planck constant and T the temperature.

Data availability All data that led us to the conclusions presented here are available with the paper or from the corresponding authors on reasonable request.

Acknowledgements We thank Shell Global Solution International B.V. for financial support. We thank Dennis Roelofszen (Shell) for consulting on technical details. Dr. Nicolas Kaeffer (MPI CEC) and Dr. Sourav Chatterjee (ETHZ) are acknowledged for fruitful discussions. Giovanni Cossu (ETHZ) is acknowledged for discussions and support regarding XPS. We thank the Mougel group (ETHZ) for access to XPS measurements. This work was carried out in part within the NCCR catalysis (financial support to the Stark group). P.-A. Payard and Q. Pessemesse are grateful to the Ecole Normale Supérieure de Lyon, Université Lyon 1 and the Region Auvergne Rhone Alpes for financial support and would like to thank Dr. Lionel Perrin (Univ Lyon) for precious advice and discussion. P.-A. P. and Q. P. are grateful to the CCIR of ICBMS, PSMN, GENCI-TGCC (Grants A0100812501 and A0120813435) for providing computational resources and technical support.

Author contributions S.B.X.Y.Z. performed all experiments and catalytic tests, measured pXRD, XPS, was involved in the development of the computational method and led the writing process. Q.P. performed metadynamics simulations under guidance of PA.P.. L.L. measured NMR. K.E. synthesized WO_3. All authors contributed to the design of the project, data interpretation and writing.

Competing interests The authors declare no competing interests.

Additional information Correspondence and requests for materials should be addressed to PA.P. and C.C.

References

(1) Hwu, H. H.; Chen, J. G. Surface chemistry of transition metal carbides. *Chem. Rev.* **2005**, *105*, 185-212. DOI: 10.1021/cr0204606.

(2) Levy, R. B.; Boudart, M. Platinum-Like Behavior of Tungsten Carbide in Surface Catalysis. *Science* **1973**, *181*, 547-549.

(3) Deng, Y.; Ge, Y.; Xu, M.; Yu, Q.; Xiao, D.; Yao, S.; Ma, D. Molybdenum Carbide: Controlling the Geometric and Electronic Structure of Noble Metals for the Activation of O−H and C−H Bonds. **2019**. DOI: 10.1021/acs.accounts.9b00182.

(4) Anasori, B.; Lukatskaya, M. R.; Gogotsi, Y. 2D metal carbides and nitrides (MXenes) for energy storage. *Nat. Rev. Mat.* **2017**, *2*, 16098. DOI: 10.1038/natrevmats.2016.98.

(5) Xiong, Z.-T.; Chen, L.-L.; Zhang, H.-B.; Zeng, J.-L.; Lin, G.-D. Study of W/HZSM-5-Based Catalysts for Dehydro-aromatization of CH4 in Absence of O2. I. Performance of Catalysts. *Catal. Lett.* **2001**, *74* (3), 227-232.

(6) Gao, J.; Zheng, Y.; Jehng, J.-M.; Tang, Y.; Wachs, I. E.; Podkolzin, S. G. Identification of molybdenum oxide nanostructures on zeolites for natural gas conversion. *Science* **2015**, *348* (6235), 686-690.

(7) Dixit, G. K.; Kumar, M.; Katiyar, A.; Jansen, A. P.; van Bavel, A. P.; Agrawal, R.; Shenai, P. M.; Srinivasan, V. Unraveling the activity of iron carbide clusters embedded in silica for thermocatalytic conversion of methane. *Catal. Sci. Technol.* **2021**, *11* (22), 7398-7411.

(8) Geng, C.; Weiske, T.; Li, J.; Shaik, S.; Schwarz, H. Intrinsic Reactivity of Diatomic 3d Transition-Metal Carbides in the Thermal Activation of Methane: Striking Electronic Structure Effects. *J. Am. Chem. Soc.* **2019**, *141*, 599-610. DOI: 10.1021/jacs.8b11739.

(9) Roman-Leshkov. Self Assembly of Noble Metal Monolayers on transition metal carbide nanoparticle catalysts. *Science* **2016**, *12*, 6397-6406. DOI: 10.1039/b000000x.

(10) Schwach, P.; Pan, X.; Bao, X. Direct Conversion of Methane to Value-Added Chemicals over Heterogeneous Catalysts: Challenges and Prospects. *Chem. Rev.* **2017**, *117*, 8497-8520. DOI: 10.1021/acs.chemrev.6b00715.

(11) Nguyen, T. N.; Nhat, T. T. P.; Takimoto, K.; Thakur, A.; Nishimura, S.; Ohyama, J.; Miyazato, I.; Takahashi, L.; Fujima, J.; Takahashi, K. High-throughput experimentation and catalyst informatics for oxidative coupling of methane. *ACS Catal.* **2019**, *10* (2), 921-932.

(12) Wang, L.; Tao, L.; Xie, M.; Xu, G.; Huang, J.; Xu, Y. Dehydrogenation and aromatization of methane under non-oxidizing conditions. *Catal. Lett.* **1993**, *21*, 35-41.

(13) Wang, D.; Lunsford, J. H.; Rosynek, M. P. Characterization of a Mo/ZSM-5 catalyst for the conversion of methane to benzene. *J. Catal.* **1997**. DOI: 10.1006/jcat.1997.1712.

(14) Murugappan, K.; Anderson, E. M.; Teschner, D.; Jones, T. E.; Skorupska, K.; Román-Leshkov, Y. Operando NAP-XPS unveils differences in MoO3 and Mo2C during hydrodeoxygenation. *Nat. Catal.* **2018**, *1*, 960-967. DOI: 10.1038/s41929-018-0171-9.

(15) Vollmer, I.; Kosinov, N.; Szécsényi, Á.; Li, G.; Yarulina, I.; Abou-hamad, E.; Gurinov, A.; Ould-chikh, S.; Aguilar-tapia, A.; Hazemann, J.-l.; et al. A site-sensitive quasi-in situ strategy to characterize Mo / HZSM-5 during activation. *J. Catal.* **2019**, *370*, 321-331. DOI: 10.1016/j.jcat.2019.01.013.

(16) Ding, W.; Li, S.; Meitzner, G. D.; Iglesia, E. Methane conversion to aromatics on Mo/H-ZSM5: structure of molybdenum species in working catalysts. *J. Phys. Chem. B* **2001**, *105*, 506-513. DOI: 10.1021/jp0030692.

(17) Choudhary, T. V.; Aksoylu, E.; Goodman, D. W. Nonoxidative Activation of Methane. *Catal. Rev. - Sci. Eng.* **2003**, *45*, 151-203. DOI: 10.1081/CR-120017010.

(18) Kim, S. K.; Kim, H. W.; Han, S. J.; Lee, S. W.; Shin, J.; Kim, Y. T. Mechanistic and microkinetic study of non-oxidative methane coupling on a single-atom iron catalyst. *Commun. Chem.* **2020**, *3*, 1-8. DOI: 10.1038/s42004-020-0306-1.

(19) Puente-Urbina, A.; Pan, Z.; Paunović, V.; Šot, P.; Hemberger, P.; Bokhoven, J. A. Direct Evidence on the Mechanism of Methane Conversion under Non-oxidative Conditions over Iron-modified Silica: The Role of Propargyl Radicals Unveiled. *Angew. Chem. Int. Ed.* **2021**, 1-6. DOI: 10.1002/anie.202107553.
(20) Vogt, C.; Meirer, F.; Monai, M.; Groeneveld, E.; Ferri, D.; van Santen, R. A.; Nachtegaal, M.; Unocic, R. R.; Frenkel, A. I.; Weckhuysen, B. M. Dynamic restructuring of supported metal nanoparticles and its implications for structure insensitive catalysis. *Nat. Commun.* **2021**, *12* (1), 1-10.
(21) Vollmer, I.; Van Der Linden, B.; Ould-Chikh, S.; Aguilar-Tapia, A.; Yarulina, I.; Abou-Hamad, E.; Sneider, Y. G.; Olivos Suarez, A. I.; Hazemann, J. L.; Kapteijn, F.; et al. On the dynamic nature of Mo sites for methane dehydroaromatization. *Chem. Sci.* **2018**, *9*, 4801-4807. DOI: 10.1039/c8sc01263f.
(22) Doornkamp, C.; Ponec, V. The universal character of the Mars and Van Krevelen mechanism. *J. Mol. Catal. A Chem.* **2000**, *162*, 19-32. DOI: 10.1016/S1381-1169(00)00319-8.
(23) Mars, P.; Van Krevelen, D. W. Oxidations carried out by means of vanadium oxide catalysts. *Chem. Eng. Sci.* **1954**, *3*, 41-59.
(24) Solymosi, F.; Cserényi, J.; Szöke, A.; Bánsági, T.; Oszkó, A. Aromatization of methane over supported and unsupported Mo-based catalysts. *J. Catal.* **1997**. DOI: 10.1006/jcat.1997.1478.
(25) Kalha, C.; Ratcliff, L. E.; Moreno, J. G.; Mohr, S.; Mantsinen, M.; Fernando, N. K.; Thakur, P. K.; Lee, T.-L.; Tseng, H.-H.; Nunney, T. S. Lifetime effects and satellites in the photoelectron spectrum of tungsten metal. *Phys. Rev. B* **2022**, *105* (4), 045129.
(26) Yang, J.; Ma, D.; Deng, F.; Luo, Q.; Zhang, M.; Bao, X.; Ye, C. Solid state 13C NMR studies of methane dehydroaromatization reaction on Mo/HZSM-5 and W/HZSM-5 catalysts. *Chem. Commun.* **2002**, *8*, 3046-3047. DOI: 10.1039/b206010h.
(27) De Souza, F. A. L.; Ambrozio, A. R.; Souza, E. S.; Cipriano, D. F.; Scopel, W. L.; Freitas, J. C. C. NMR spectral parameters in graphene, graphite, and related materials: Ab initio calculations and experimental results. *J. Phys. Chem. C* **2016**, *120*, 27707-27716. DOI: 10.1021/acs.jpcc.6b10042.
(28) Laio, A.; Parrinello, M. Escaping free-energy minima. *Proc. Natl. Acad. Sci.* **2002**, *99* (20), 12562-12566.
(29) Barducci, A.; Bonomi, M.; Parrinello, M. Metadynamics. *Comput. Mol. Sci.* **2011**, *1* (5), 826-843.
(30) Barducci, A.; Bussi, G.; Parrinello, M. Well-tempered metadynamics: a smoothly converging and tunable free-energy method. *Phys. Rev. Lett.* **2008**, *100* (2), 020603.
(31) Valsson, O.; Tiwary, P.; Parrinello, M. Enhancing important fluctuations: Rare events and metadynamics from a conceptual viewpoint. *Annu. Rev. Phys. Chem.* **2016**, *67* (1), 159-184.
(32) Bussi, G.; Branduardi, D. Free-energy calculations with metadynamics: Theory and practice. *Rev. Comput. Chem.* **2015**, *28*, 1-49.
(33) Yaws, C. L. Diffusion coefficient in water–organic compounds. In *Transport properties of chemicals and hydrocarbons*, Elsevier, 2009; pp 502-593.
(34) Zhang, T.; Holiharimanana, D.; Yang, X.; Ge, Q. DFT Study of Methane Activation and Coupling on the (0001) and (112^{-}0) Surfaces of α-WC. *J. Phys. Chem. C* **2020**. DOI: 10.1021/acs.jpcc.0c06928.
(35) Carstens, J. N.; Bell, A. T. Methane activation and conversion to higher hydrocarbons on supported ruthenium. *J. Catal.* **1996**, *161*, 423-429. DOI: 10.1006/jcat.1996.0200.
(36) Razdan, N. K.; Bhan, A. Carbidic Mo is the sole kinetically-relevant active site for catalytic methane dehydroaromatization on Mo / H-ZSM-5. *J. Catal.* **2020**, *389*, 667-676. DOI: 10.1016/j.jcat.2020.06.035.
(37) Eng, J.; Chen, J. G.; Abdelrehim, I. M.; Madey, T. E. Vibrational study of the interaction of acetylene and benzene on clean and carbide-modified W(211) surfaces. *J. Phys. Chem. B* **1998**, *102*, 9687-9696. DOI: 10.1021/jp9826120.
(38) Siaj, M.; Oudghiri-Hassani, H.; Maltais, C.; McBreen, P. H. Thermally stable alkylidene groups on the surface of β-Mo 2C: Relevance to methane aromatization and olefin-metathesis catalysis. *J. Phys. Chem. C* **2007**, *111*, 1725-1732. DOI: 10.1021/jp064599m.
(39) Ordomsky, V. V.; Legras, B.; Cheng, K.; Paul, S.; Khodakov, A. Y. The role of carbon atoms of supported iron carbides in Fischer-Tropsch synthesis. *Catal. Sci. Technol.* **2015**, *5*, 1433-1437. DOI: 10.1039/c4cy01631a.

(40) Ding, W.; Meitzner, G. D.; Marler, D. O.; Iglesia, E. Synthesis, Structural Characterization, and Catalytic Properties of Tungsten-Exchanged H-ZSM5 *J. Phys. Chem. B* **2001**. DOI: 10.1021/jp003413v.
(41) Vollmer, I.; Yarulina, I.; Kapteijn, F.; Gascon, J. Progress in Developing a Structure-Activity Relationship for the Direct Aromatization of Methane. *ChemCatChem* **2019**, *11*, 39-52. DOI: 10.1002/cctc.201800880.
(42) Deng, M.; Qi, J.; Li, X.; Xiao, Y.; Yang, L.; Yu, X.; Wang, H.; Yuan, B.; Gao, Q. MoC/C nanowires as high-rate and long cyclic life anode for lithium ion batteries. *Electrochim. Acta* **2018**, *277*, 205-210. DOI: 10.1016/j.electacta.2018.04.185.
(43) Kühne, T. D.; Iannuzzi, M.; Del Ben, M.; Rybkin, V. V.; Seewald, P.; Stein, F.; Laino, T.; Khaliullin, R. Z.; Schütt, O.; Schiffmann, F. CP2K: An electronic structure and molecular dynamics software package-Quickstep: Efficient and accurate electronic structure calculations. *J. Chem. Phys.* **2020**, *152* (19), 194103.
(44) Hutter, J.; Iannuzzi, M.; Schiffmann, F.; VandeVondele, J. cp2k: atomistic simulations of condensed matter systems. *Comput. Mol. Sci.* **2014**, *4* (1), 15-25.
(45) Parthé, E.; Sadogopan, V. The structure of dimolybdenum carbide by neutron diffraction technique. *Acta Crystallogr.* **1963**, *16* (3), 202-205.
(46) Page, K.; Li, J.; Savinelli, R.; Szumila, H. N.; Zhang, J.; Stalick, J. K.; Proffen, T.; Scott, S. L.; Seshadri, R. Reciprocal-space and real-space neutron investigation of nanostructured Mo2C and WC. *Solid State Sci.* **2008**, *10* (11), 1499-1510.
(47) Perdew, J. P.; Burke, K.; Ernzerhof, M. Generalized gradient approximation made simple. *Phys. Rev. Lett.* **1996**, *77* (18), 3865.
(48) Zhang, Y.; Yang, W. Comment on "Generalized gradient approximation made simple". *Phys. Rev. Lett.* **1998**, *80* (4), 890.
(49) Grimme, S.; Antony, J.; Ehrlich, S.; Krieg, H. A consistent and accurate ab initio parametrization of density functional dispersion correction (DFT-D) for the 94 elements H-Pu. *J. Chem. Phys.* **2010**, *132* (15), 154104.
(50) Grimme, S.; Ehrlich, S.; Goerigk, L. Effect of the damping function in dispersion corrected density functional theory. *J. Comput. Chem.* **2011**, *32* (7), 1456-1465.
(51) Lippert, B. G.; Parrinello, J. H.; Michele. A hybrid Gaussian and plane wave density functional scheme. *Mol. Phys.* **1997**, *92* (3), 477-488.
(52) VandeVondele, J.; Hutter, J. Gaussian basis sets for accurate calculations on molecular systems in gas and condensed phases. *J. Chem. Phys.* **2007**, *127* (11), 114105.
(53) Krack, M. Pseudopotentials for H to Kr optimized for gradient-corrected exchange-correlation functionals. *Theor. Chem. Acc.* **2005**, *114* (1), 145-152.
(54) Kürpick, U.; Kara, A.; Rahman, T. S. Role of lattice vibrations in adatom diffusion. *Phys. Rev. Lett.* **1997**, *78* (6), 1086.